LAWRENCE
LIVERMORE
NATIONAL
LABORATORY

LLNL-CONF-599093

A RADIATING SHOCK EVALUATED USING IMPLICIT MONTE CARLO DIFFUSION

M. Cleveland, N. Gentile

November 6, 2012

The International Conference on Mathematics and Computational Methods Applied to Nuclear Science and Engineering
Sun Valley, ID, United States
May 5, 2013 through May 9, 2013

Disclaimer

International Conference on Mathematics and Computational Methods Applied to Nuclear Science & Engineering (M&C 2013)
Sun Valley, Idaho, USA, May 5-9, 2013, on CD-ROM, American Nuclear Society, LaGrange Park, IL (2013)

A RADIATING SHOCK EVALUATED USING IMPLICIT MONTE CARLO DIFFUSION

Mathew Cleveland and Nick Gentile *
Lawrence Livermore National Laboratory
L-405, P. O. Box 808, Livermore California 94550
cleveland7@llnl.gov; gentile1@llnl.gov

ABSTRACT

Implicit Monte Carlo [1] (IMC) has been shown to be very expensive when used to evaluate a radiation field in opaque media. Implicit Monte Carlo Diffusion (IMD) [2], which evaluates a spatial discretized diffusion equation using a Monte Carlo algorithm, can be used to reduce the cost of evaluating the radiation field in opaque media [2]. This work couples IMD to the hydrodynamics equations to evaluate opaque diffusive radiating shocks. The Lowrie semi-analytic diffusive radiating shock benchmark [3] is used to verify our implementation of the coupled system of equations.

Key Words: Implicit Monte Carlo Diffusion, Radiating Shock

1. INTRODUCTION

This work extends Implicit Monte Carlo Diffusion (IMD) to be used in the evaluation of coupled fluid-frame radiation hydrodynamics simulations in opaque media. The original semi-implicit discretization of the radiative transfer equations developed by Fleck and Cummings [1] can accurately resolve radiation fields without a non-linear iteration. This set of semi-implicit equations creates "effective scattering" which represents the absorption and re-emission of photons over a time step. In opaque media, the effective scattering can begin to dominate particle interactions. In these thick scattering regions of a problem, standard IMC becomes prohibitively expensive. As a result, many methods have been developed to accelerate the solution of these equations in opaque materials [2,4,5].

Asymptotic analysis has shown that diffusion can accurately predict the radiative transport solution in a thick diffuse limit [6]. Implicit Monte Carlo Diffusion (IMD) [2] solves the semi-implicit radiative diffusion equations using a Monte Carlo approach. This is done by developing interaction probabilities which have physical interpretations from the spatial discretized set of implicit radiative diffusion equations[7].

Most realistic problems contain both opaque and transparent material. These thick and thin regions of a problem can exist both in the space and frequency domain. The strong similarities between IMC and IMD make them ideal candidates to hybridize, using IMC in the streaming regions and IMD in the diffusive regions. This has similarly been shown using IMC and Discrete Diffusion Monte Carlo (DDMC) [4]. The DDMC and IMD methods are nearly identical and only vary in temporal discretizations. DDMC is continuous in time as compared to IMD that is discrete in time.

*LLNL-CONF-599093

2. CONSERVATION EQUATIONS

The frequency-independent fluid-frame radiation hydrodynamic equations can be written as [8]:

$$\frac{D\rho}{Dt} + \rho\nabla \cdot u = 0 \tag{1}$$

$$\rho\frac{Du}{Dt} + \nabla\left(p + p_r\right) = 0 \tag{2}$$

$$\rho\frac{D\epsilon_m}{Dt} + \frac{1}{2}\rho\frac{Du}{Dt} + \nabla \cdot pu = c\kappa_a f E - ca\kappa_a f T_m^4 \tag{3}$$

$$\frac{DE}{Dt} + E\nabla \cdot u + \nabla \cdot F + p_r\nabla \cdot u = ca\kappa_a f T_m^4 - c\kappa_a f E \tag{4}$$

where the Fleck and Cummings [1] first order expansion of the emission source has been applied to the radiation equations. The notation $\frac{D}{Dt}$ refers to a Lagrangian, as apposed to a Eulerian $\frac{\partial}{\partial t}$, time derivative.

This tightly coupled set of equations accounts for the conservation of mass (Eq. 1), the conservation of momentum (Eq. 2), the conservation of material energy (Eq. 3), and the conservation of photon energy (Eq. 4). The variables in these equations are as follows: ρ is the material density, u is the material velocity, p is the material pressure, E is the gray photon energy density, ϵ_m is the material energy density, c is the speed of light, a is the radiation constant, κ is the gray material opacity where the subscripts a and t denote the absorption and total opacity, f is the Fleck factor [1], and T_m is the material temperature. In this work, we have made the assumption that the radiation momentum deposition can be approximated using the radiation pressure (p_r). This is known as the Eddington approximation [8]:

$$p_r = \frac{1}{3}E \tag{5}$$

This assumption allows for simple momentum deposition evaluation for both IMC and IMD. However, it is only valid if the radiation energy density is linearly anisotropic [8]. More sophisticated approaches for radiation momentum deposition treatment for diffusion have been proposed by Densmore et al. [4].

2.1. Fluid Frame Radiative Diffusion

The radiation advection terms present in the conservation of photon energy (Eq. 4) are evaluated via operator splitting [8]. The conservation of radiation energy (Eq. 4) is operator split into the radiation interactions,

$$\frac{DE}{Dt} + \nabla \cdot F = ca\kappa_a f T_m^4 - c\kappa_a f E \tag{6}$$

and the work done to the radiation field by the flow.

$$\frac{DE}{Dt} + \frac{4}{3}E\nabla \cdot u = 0 \tag{7}$$

The material energy conservation equation is also operator split to evaluate the radiation-material energy exchange

$$\rho\frac{D\epsilon_m}{Dt} = c\kappa_a f E - ca\kappa_a f T_m^4 \tag{8}$$

separately from the other material energy conservation terms.

$$\rho\frac{D\epsilon_m}{Dt}+\frac{1}{2}\rho\frac{Du}{Dt}+p\nabla\cdot u=0 \tag{9}$$

Applying the diffusion approximation, with the assumption that the material properties are homogeneous in individual cells, to Eq. 6 and integrating over volume yields the standard form of the discretized radiation diffusion equation [9]:

$$(E_i^{n+1}-E_i^n)\Delta V_i-c\sum_f^N A_f D_f\nabla E_f\Delta t=ca\kappa_{a_i}f_i{T_{m_i}^n}^4\Delta V_i\Delta t-c\kappa_{a_i}f_iE_i^{n+1}\Delta V_i\Delta t, \tag{10}$$

where D_f and A_f are the average diffusion coefficient and area for a face and the subscript i denotes variables at the cell center. Assuming a 1D mesh, the face averaged diffusion coefficient for a second order finite volume discretization can be expressed as [9]:

$$D_f=\frac{D_{f+\frac{1}{2}}D_{f-\frac{1}{2}}(X_{f+\frac{1}{2}}-X_{f-\frac{1}{2}})}{D_{f+\frac{1}{2}}(X_f-X_{f-\frac{1}{2}})+D_{f-\frac{1}{2}}(X_{f+\frac{1}{2}}-X_f)}, \tag{11}$$

where X is a position in space, and the subscript f denotes a face value and $(f+\frac{1}{2})$ and $(f-\frac{1}{2})$ denote cell centered values on either side of the face.

The selection of the face averaged diffusion coefficient for this discretization scheme is important, because very thick cells can unphysically stop photon propagation when adjoined by relatively thin cells [9]. This can be prevented, when the opacities are strongly temperature dependent, by weighting the face averaged diffusion coefficients with the material temperature. This weighting is such that the diffusion coefficient always favors the hot (or thin) material opacity:

$$D'_{f+\frac{1}{2}}=D_{f+\frac{1}{2}}\frac{T^4_{f+\frac{1}{2}}+T^4_{f-\frac{1}{2}}}{2T^4_{f+\frac{1}{2}}}. \tag{12}$$

The new material temperature weighted face averaged diffusion coefficient can be constructed by replacing all diffusion coefficients D in Eq. 11 with the weighted diffusion coefficient D'.

2.2. Work Done to The Radiation Field

The equation for the work done to the radiation field (Eq. 7) can be transformed from a spatial derivative of the velocity to a Lagrangian time derivative of the volume V.

$$\frac{DE}{Dt}+\frac{4}{3}\frac{E}{V}\frac{DV}{Dt}=0 \tag{13}$$

Integrating this newly transformed equation over a time step results in the change in energy density associated with the work done to the radiation field by the fluid:

$$E_i^{n+1}=E_i^n\left(\frac{V_i^n}{V_i^{n+1}}\right)^{4/3}. \tag{14}$$

This operator splitting is executed for both IMC and IMD in this work. IMC typically tracks the work done to the radiation field and the radiation pressure directly during the Monte Carlo ray tracing. This operator splitting and the application of the Eddington approximation (Eq. 5) was done for ease and consistency between IMC and IMD.

2.3. Radiation hydrodynamics using IMD

These coupled equations are solved by first evaluating Lagrangian hydrodynamics [10]. The work added to the radiation field is evaluated using equation Eq. 14. The newly defined energy density is then used in the IMD simulation to evaluate the radiation diffusion equation.

IMD uses the discretized diffusion equation (Eq. 10) to generate a set of probabilities which describe Monte Carlo particle interactions in the system. These interaction include exchanges between the radiation field, the materials, and the mesh which define the problem. These probabilities are then used to track Monte Carlo particles. The Monte Carlo particles are sourced on to the mesh given the radiation energy emitted from the material ($ca\kappa_{a_i} f_i T^4_{m_i} \Delta V_i \Delta t$), radiation energy that exists in the cell from the previous time step ($E^n_i \Delta V_i$), and any additional external radiation sources. The resulting radiation field, which evaluated using the tallied IMD Monte Carlo particle interactions, is used to inform the hydrodynamics equations for the next time step.

3. TEST CASE

The semi-analytic radiation diffusion shock benchmark developed by Lowrie and Edwards [3] is used to verify the coupled IMD solver presented in this work. This is a radiating shock problem with a Mach number of 45. The pre-shock and post-shock conditions are listed in Table I.

Table I. Pre-shock and post-shock conditions.

Properties	Pre-Shock	Post-Shock	Units
ρ	1	6.4261	[g/cc]
u	0	-4.8175×10^8	[cm/s]
T	0.1	8.3578	[keV]

Two variations, an optically thin (simulation A) and optically thick (simulation B) version, of the problem are evaluated. The material is assumed to be a gamma law gas for both problems where gamma (γ) and specific heat values (C_v) are the same for both problems. The gamma law gas assumption provides a closure for Eq. 8. The problems are composed of homogeneous materials whose properties are listed in Tables II.

Table II. Simulation material properties.

Properties	Simulation A	Simulation B	Units
κ	$4.4940 \times 10^8 \rho T^{-3.5}$	$2.6964 \times 10^{12} \rho T^{-3.5}$	[cm^2/g]
κ_s	0.4006	40.06	[cm^2/g]
γ	5.0/3.0	5.0/3.0	Unitless
C_v	0.1447×10^{15}	0.1447×10^{15}	[erg/(g keV)]

The shock front is driven by a black body emission source with the post-shock material temperature on the right most boundary face. The initial sonic point, where the material Mach number is equal to 1, is set at $x = 2300$ [cm]. The initial shock profile for simulation A is defined as Lowrie's analytic result. The analytic solution for simulation B was not available. However, the optical thickness is so large that the radiation acts like a $\gamma = \frac{4}{3}$ ideal gas. Thus, as the optical thickness increases the analytic result converges to a step function which satisfies the Rankine-Hugoniot relations [8], where the pressure and energy density in the relations includes both matter and radiation contributions.

4. RESULTS

The simulations were evaluated using both the IMC [11] and IMD methods separately. Each simulation used 1000 initially equally spaced cells over the domain $0 \leq x \leq 2500$ [cm]. Each problem was run to a final time of 4e-8 [sec] using 1.0×10^5 particle histories per time step. The time step size is confined such that $1 \times 10^{-13} \leq \Delta t \leq 1 \times 10^{-10}$ [sec].

The material and radiation temperatures along with their analytic solution, provided by Lowrie [3], for simulation A are shown in Figs. 1 and 2. Running in serial, the IMD simulation ran 7.5 times faster than IMC. Both simulations match the analytic solution very well while the IMC solution is slightly noisier than the IMD solution.

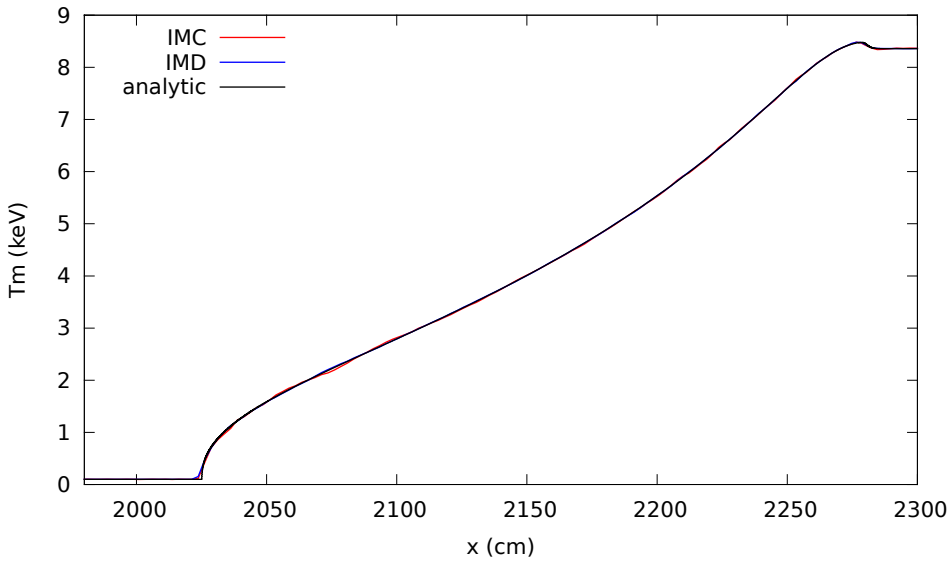

Figure 1. Material temperature (Tm) profiles for simulation A at 4e-8 [sec] as evaluated separately by the IMD and IMC algorithms compared to the analytic result

The analytic solution to the thick scattering problem, simulation B, was not available. However, the thick highly scattering opacities forces the solution to be a step function. The problem was initialized with a simple discontinuity at the initial sonic point such that all values in the domain $2300 \leq x \leq 2500$ [cm] are set to be the post-shock condition and all values in the domain $0 \leq x < 2300$ [cm] are set to the pre-shock condition. This approximation of the initial analytic solution produces a well behaved shock front. To demonstrate that the shock front is stable, the IMD simulation was run to 10×10^{-6} [sec]. Fig. 3 shows that the shock wave quickly approaches a fully developed shape as it progress through time. The shock front at

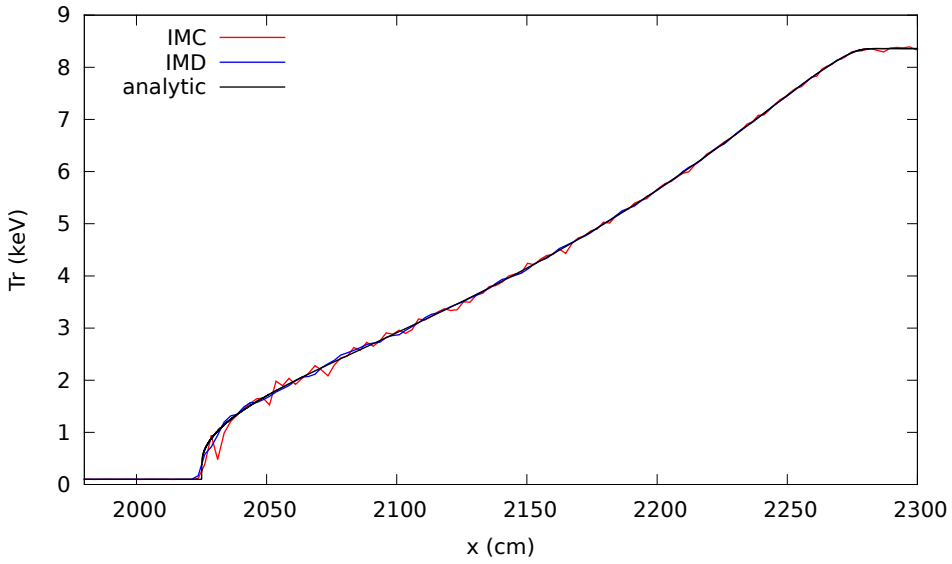

Figure 2. Radiation temperature (Tr) profiles for simulation A at 4e-8 [sec] as evaluated separately by the IMD and IMC algorithms compared to the analytic result

different time points have been translated back to the original shock location,

$$X(x, \Delta t) = x - v_s \Delta t \tag{15}$$

where v_s is the velocity of the shock.

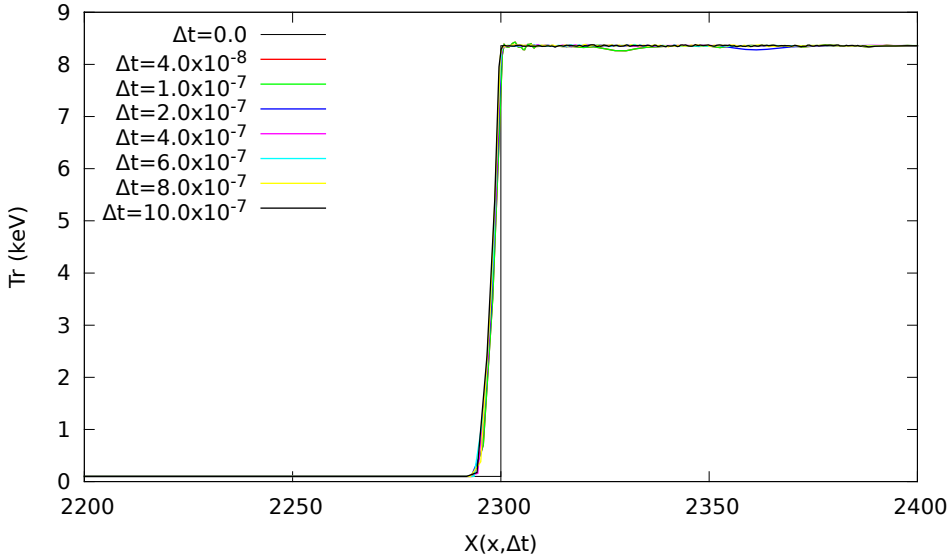

Figure 3. Translated radiation temperature profiles evaluated using IMD for simulation B at various times.

To determine the effect of neglecting the radiation pressure (Eq. 5) and work done by the hydrodynamics (Eq. 14), three different IMD simulations were compared to IMC for simulation B: a simulation that included the radiation pressure and work done by the hydrodynamics: "IMD"; a simulation that neglects the work

done by the hydrodynamics but included the radiation pressure: “IMD-NW”; and a simulation that neglected both the work done by hydrodynamics and the radiation pressure: “IMD-NWRP”. A comparison of the material temperature, velocity, and density for each of the three different IMD simulation is shown in Figures 4, 5, and 6 respectively. The “Idealized Shock” line shown in these figures is the initial hydrodynamic shock profile used at $t = 0$ translated at the analytic shock velocity. “IMD” ran 32 times faster than ”IMC” for domain replicated simulations which used 128 processors each. Including both the radiation pressure and the work done by the hydrodynamics is necessary to get agreement between IMC and IMD simulations. This can be seen in Figures 4, 5, and 6 in which IMC and IMD solutions only match in shape and location if both operators are accounted for. Neglecting either operator artificially affects the propagation and shape of the shock wave.

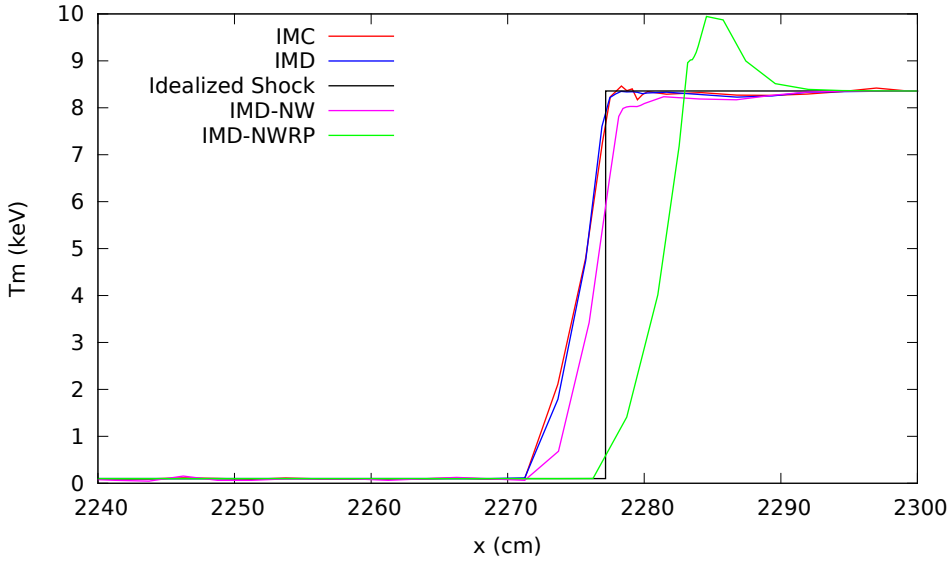

Figure 4. Material temperature profile for simulation B at 4e-8 [sec] as evaluated separately by the IMD and IMC algorithms.

5. CONCLUSIONS

This work implemented IMD into a fluid-frame radiation hydrodynamics package. This paper included a brief explanation of how the work done to the radiation field by the fluid is treated. The method was tested using a semi-analytic radiative diffusion shock problem developed by Lowrie [3]. The fact that this is an analytic diffusion solution makes it ideal for the verification of our IMD solver. It was found that the IMD method produces an accurate result to this radiating shock test case.

The radiation pressure estimates the momentum deposition from the radiation field into the material which helps drive the hydrodynamics. The work done by the hydrodynamics to the radiation field scales the magnitude of the energy density to account for cell compression by the hydrodynamics and helps insure energy conservation. Evaluating the work done by the hydrodynamics through operator splitting and approximating the radiation momentum deposition with the radiation pressure produces accurate IMD simulations for radiating shocks (see Figs. 1 and 2). It was determined that neglecting the work done by the radiation and/or the radiation pressure can lead to serious errors in the simulation of thick radiating shocks (see Fig. 4, Fig. 5, and Fig. 6). Neglecting the work done by the hydrodynamics has less of an effect on the overall accuracy of the solution as compared to neglecting the radiation pressure.

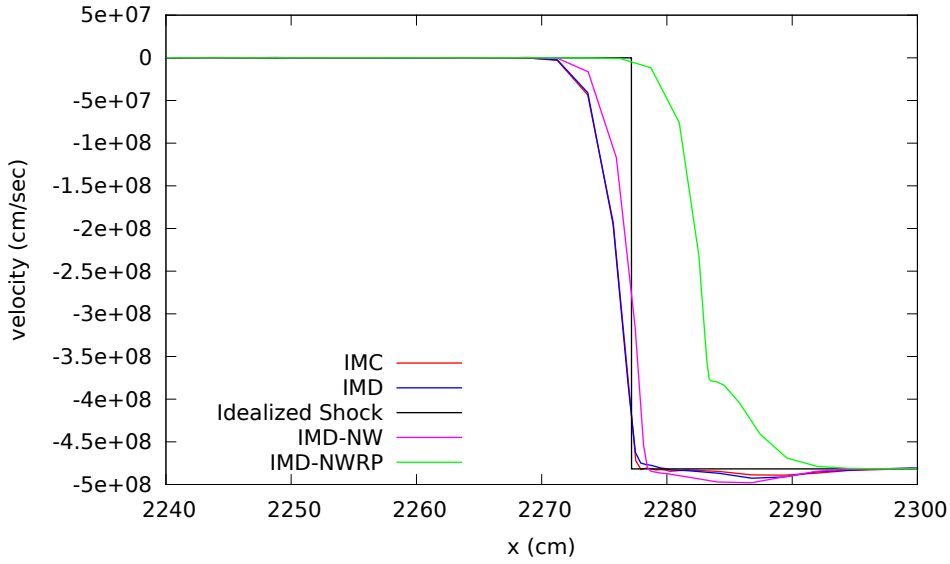

Figure 5. Material velocity profile for simulation B at 4e-8 [sec] as evaluated separately by the IMD and IMC algorithms.

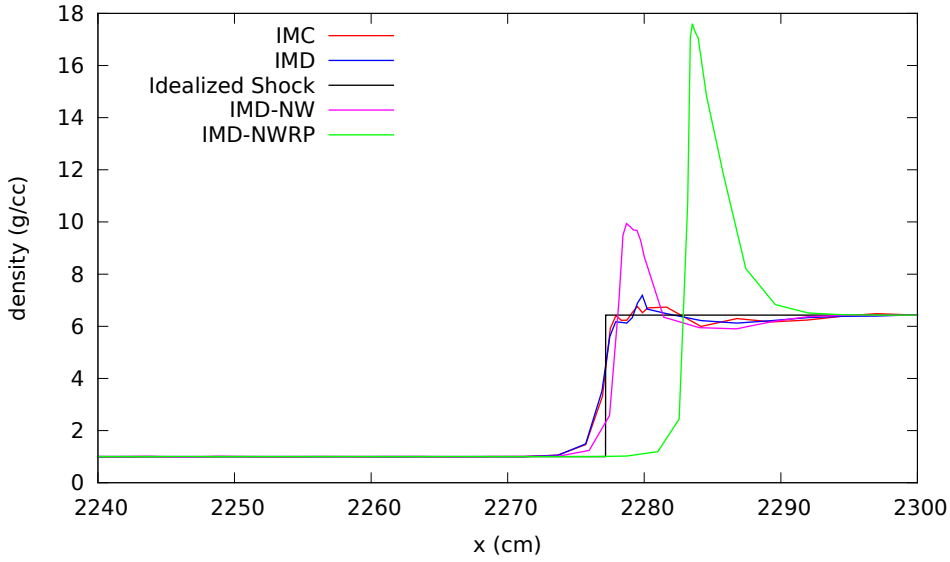

Figure 6. Material density for simulation B at 4e-8 [sec] as evaluated separately by the IMD and IMC algorithms.

IMD showed a modest speed improvement over IMC for the thinner of the two simulations ($7.5\times$ faster than IMC in simulation A) while it showed a drastic improvement for the thick simulation ($32\times$ faster than IMC in simulation B). Future work will investigate the effect of optical thickness and scattering ratios on the computational cost. This will include figure of merit calculations. The figure of merit calcuation takes into account the run time and the statistical noise of the solution. The figure of merit comparison will further highlight the advantages of IMD which has less statistical noise in diffisive regions than IMC. Future work will also include comparisons of hybrid IMC/IMD calculations.

ACKNOWLEDGEMENTS

This work was performed under the auspices of the U.S. Department of Energy by Lawrence Livermore National Laboratory under Contract DE-AC52-07NA27344.

REFERENCES

[1] J. Fleck Jr. and J. Cummings Jr., An implicit Monte Carlo scheme for calculating time and frequency dependent nonlinear radiation transport, *Journal of Computational Physics*, **8**, 3, pp. 313–342 (1971).

[2] N. Gentile, Implicit Monte Carlo Diffusion – An Acceleration Method for Monte Carlo Time-Dependent Radiative Transfer Simulations, *Journal of Computational Physics*, **172**, 2, pp. 543–571 (2001).

[3] R. Lowrie and J. Edwards, Radiative shock solutions with grey nonequilibrium diffusion, *Shock Waves*, **18**, 2, pp. 129–143 (2008).

[4] J. D. Densmore, T. J. Urbatsch, T. M. Evans, and M. W. Buksas, A hybrid transport-diffusion method for Monte Carlo radiative-transfer simulations, *Journal of Computational Physics*, **222**, 2, pp. 485–503 (2007).

[5] J. Fleck Jr. and E. Canfield, A random walk procedure for improving the computational efficiency of the implicit Monte Carlo method for nonlinear radiation transport, *Journal of Computational Physics*, **54**, 3, pp. 508–523 (1984).

[6] E. Larsen, G. Pomraning, and V. Badham, Asymptotic analysis of radiative transfer problems, *Journal of Quantitative Spectroscopy and Radiative Transfer*, **29**, 4, pp. 285–310 (1983).

[7] M. A. Cleveland, N. A. Gentile, and T. S. Palmer, An extension of implicit Monte Carlo diffusion: Multigroup and the difference formulation, *Journal of Computational Physics*, **229**, 16, pp. 5707–5723 (2010).

[8] J. I. Castor, *Radiation Hydrodynamics*, Cambridge University Press (2007).

[9] R. Szilard and G. Pomraning, *Numerical transport and diffusion methods in radiative transfer* (1992).

[10] E. Caramana, D. Burton, M. Shashkov, and P. Whalen, The Construction of Compatible Hydrodynamics Algorithms Utilizing Conservation of Total Energy, *Journal of Computational Physics*, **146**, 1, pp. 227–262 (1998).

[11] N. A. Gentile, N. Keen, and J. Rathkopf, The Kull IMC package, Tech. rep., Tech. Rep. UCRL-JC-132743, Lawrence Livermore National Laboratories, Livermore, CA (1998).